

A New Mathematical Model of Laser Percussion Drilling

Suchatawat M.

Department of Mechanical Engineering, Faculty of Engineering, King Mongkut's Institute of Technology,
Ladkrabang, Bangkok, Thailand 10520
ksmaturo@kmitl.ac.th, tel. (+44) 2-329-8350, fax. (+44) 2-329-8352

Abstract

Laser percussion drilling is widely used for producing cooling holes in aerospace engine components. In order to maximise the cooling efficiency, the laser drilled holes need to be produced to a high degree of accuracy and with least defects. This paper presents a new mathematical model of laser percussion drilling which takes into account the recoil pressure exerted on the molten liquid surface, and the exothermic energy generated from oxidation of the liquid metal and O₂ assist gas. The analysis is based on transient heat conduction in solid and liquid regions with appropriate boundary and initial conditions at the solid-liquid and liquid-vapour interfaces. The new model enables the prediction of the hole depth and hole profile. It is found that the laser peak power and pulse width are shown to have a significant influence over the hole depth whereas the changes due to assist gas pressure are less pronounced.

Keywords: laser percussion drilling, laser drilling model, solidification.

1. Introduction

Laser drilling has become a reliable option for a wide variety of industrial applications. Of particular interest is laser drilling of cooling holes for aerospace engine components [1-3]. This is due to its ability to precisely produce small, shaped holes in difficult-to-machine materials, with high processing speed and repeatability [4-6]. Laser drilling can be processed by means of single pulse, trepanning, percussion or helical drilling techniques. Single pulse drilling is generally used for drilling a thin sheet of material. Trepanning and helical drilling give better quality holes but require longer processing time [7, 8]. Laser percussion drilling is considered as a prime candidate for applications where a large number of small precision holes with high aspect ratio are to be drilled.

Numerous laser percussion drilling models and simulation algorithms have been proposed to date with an attempt to describe the role of each phenomenon in the drilling process and to determine the optimal parameters for particular applications [9-13]. Literature review shows that most laser percussion drilling models previously developed are typically based on heat conduction, melting, and vaporization equations with a set of defined assumptions. However, most works either ignore the effects of the additional heat generated from exothermic reaction which in fact has great influence on the drilling mechanisms. This indicates that the accuracy of the available

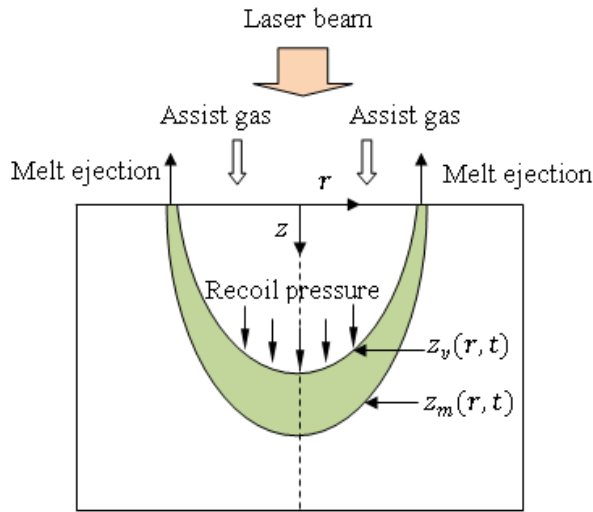
models can be considerably improved by reducing the number of assumptions and by incorporating more related phenomena into the calculations.

In this paper, a new mathematical model for multiple pulsed laser drilling is developed. The model accounts for the recoil pressure and the exothermic energy. The governing equations are set up from heat conduction, energy, and mass equations at the solid-liquid and liquid-vapour interfaces. Solutions are obtained using Mathematica 7 as a tool to solve the system of non-linear equations.

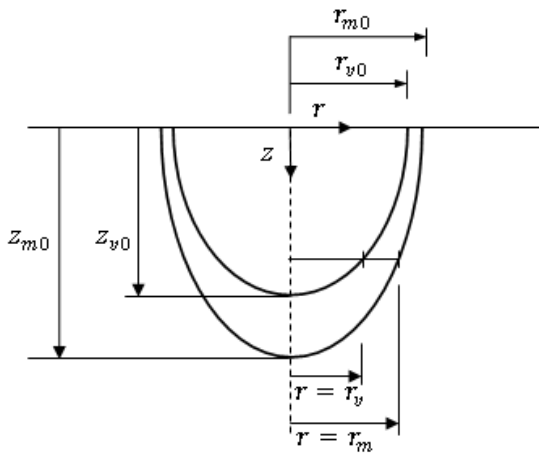
2. Mathematical model

A schematic diagram of the model is illustrated in Fig. 1(a). A laser beam with intensity I_0 irradiates the substrate surface which is initially at temperature T_0 . The solid substrate is then heated, melted and vaporized. Once the vapour is formed, it exerts recoil pressure on the molten liquid as it leaves the cavity, and pushes the melt away radially. The material removal therefore consists of two mechanisms; vaporization and melt ejection. Oxygen assist gas also plays some role in the process. The oxidation reaction between oxygen and metal provides the additional energy, called exothermic energy, to the laser beam-material interaction. The assist gas also enhances the melt ejection mechanism by adding more pressure to the recoil pressure. Moreover, the assist gas also promotes heat

convection rate at the surface of the liquid layer. Fig. 1(b) illustrates variables defined in the model.



(a)



(b)

Figs. 1 (a) Schematic diagram of the model,
(b) variables defined in the model.

Following assumptions are made for the model:

1. The absorbed laser intensity distribution over the workpiece surface is assumed to be uniform. This assumption is reasonable because the laser beam considered is produced by the Nd:YAG laser and is delivered through a fibre with an approximately top hat profile [14].
2. Plasma generation is neglected in the model. It is valid to assume so because, unlike the CO₂ laser, in case of Nd:YAG laser operating at 1.06 μm , the plasma may not be formed during the drilling process [14-16].
3. No interaction between laser beam and the vapour. It is considered here that the vapour is

optically thin, hence no laser power is absorbed. Moreover, assist gas employed also help to remove the vapour from the cavity.

4. No laser power is absorbed by the ejected melt.
5. The generation of shock waves is ignored.
6. The changes in surface absorptivity, melting point, and boiling point due to oxide layer formed are neglected. The competing effects between the possible change in the absorptivity and the difference in the melting and boiling points of the oxide and parent material are assumed to cancel each other.
7. Not all of the metal oxidises with O₂ assist gas. The oxidation efficiency is introduced in the model.
8. The discontinuity between the vapour above the liquid surface and the liquid is negligible. That is, the vapour and liquid at the surface are in thermodynamic equilibrium.

2.1 Energy balance

Once the vaporization has started, the liquid-vapour and solid-liquid interfaces are formed, respectively, at

$$z = z_v(r, t) \quad (1)$$

$$z = z_m(r, t) \quad (2)$$

where $z_v(r, t)$ and $z_m(r, t)$ are the vaporization and melting fronts, r and t are radial distance and time. At the liquid-vapour interface, the Stefan equation can be written as:

$$\rho_l L_v \frac{\partial z_v}{\partial t} - k_l \frac{\partial T_l}{\partial z} \left[1 + \left(\frac{\partial z_v}{\partial r} \right)^2 \right] =$$

$$I_{abs} + \rho_l H_{ox} \eta_{ox} \frac{\partial z_m}{\partial t} - h_g (T_{l0} - T_g) \quad (3)$$

where ρ_l , k_l and L_v are liquid density, thermal conductivity of liquid and latent heat of vaporization, I_{abs} , H_{ox} , η_{ox} , and h_g are absorbed laser intensity, enthalpy of oxidation, oxidation efficiency and heat transfer coefficient of assist gas, T_l , T_g and T_{l0} are temperature of the melt, assist gas, and melt surface, respectively.

The heat transfer coefficient h_g , is required for calculating the convection heat loss in Eq.(3). In case of forced convection, h_g can be determined from [14]:

$$h_g = \frac{k_g}{2r_{v0}} \left(C_c \text{Re}^{n_c} \text{Pr}^{1/3} \right) \quad (4)$$

where r_{v0} is the radius of the liquid-vapour interface (vapour front radius) at the hole

entrance, k_g , Re , and Pr are the thermal conductivity, Reynolds number, and Prandtl number of the assist gas, respectively, C_c and n_c are the constants for forced convection perpendicular to the liquid surface, and are taken to be 0.228 and 0.731 [17], respectively. The Reynolds number, Re , is expressed as:

$$Re = \frac{\rho_g v_g 2r_{v0}}{\mu_g} \quad (5)$$

where ρ_g , v_g , and μ_g are the density, flow velocity, and dynamic viscosity of the assist gas, respectively.

The Stefan equation for the solid-liquid interface can be written as:

$$\rho_s L_m \frac{\partial z_m}{\partial t} = \left(k_s \frac{\partial T_s}{\partial z} - k_l \frac{\partial T_l}{\partial z} \right) \left[1 + \left(\frac{\partial z_m}{\partial r} \right)^2 \right] \quad (6)$$

where ρ_s , k_s and T_s are density of solid, thermal conductivity of solid, and temperature of the solid, respectively.

At the symmetry axis, $\frac{\partial z_m}{\partial r} = 0$ and $\frac{\partial z_v}{\partial r} = 0$,

and hence the Stefan equations at the two interfaces can be rewritten as:

$$\rho_l L_v \frac{\partial z_v}{\partial t} - k_l \frac{\partial T_l}{\partial z} = I_{abs} + \rho_l H_{ox} \eta_{ox} \frac{\partial z_m}{\partial t} - h_g (T_{l0} - T_g) \quad (7)$$

$$\rho_s L_m \frac{\partial z_m}{\partial t} = \left(k_s \frac{\partial T_s}{\partial z} - k_l \frac{\partial T_l}{\partial z} \right) \quad (8)$$

According to the actual drilled hole geometry, $z_m(r,t)$ and $z_v(r,t)$ may be assumed to have parabolic profiles, i.e.

$$z_m(r,t) = z_{m0}(t) - \frac{r^2}{r_{m0}^2} z_{m0}(t) \quad (9)$$

$$z_v(r,t) = z_{v0}(t) - \frac{r^2}{r_{v0}^2} z_{v0}(t) \quad (10)$$

where $z_{m0}(t)$ and $z_{v0}(t)$ are the melt depth and vaporization depth at $r = 0$ and r_{m0} is the radius of the solid-liquid interface (melt front radius) at the hole entrance, respectively.

By substituting Eqs.(9) and (10) into Eqs.(7) and (8), and further assuming linear temperature profiles in the thin layers of liquid and solid, Stefan conditions at the two interfaces may be expressed as:

$$\rho_l L_v \frac{dz_{v0}(t)}{dt} - k_l \frac{T_m - T_{l0}}{z_{m0}(t) - z_{v0}(t)} = I_{abs} + \rho_l H_{ox} \eta_{ox} \frac{dz_{m0}(t)}{dt} - h_g (T_{l0} - T_g) \quad (11)$$

$$\rho_s L_m \frac{dz_{m0}(t)}{dt} = k_s \frac{(T_m / e) - T_m}{2\sqrt{\alpha_s t}} - k_l \frac{T_m - T_{l0}}{z_{m0}(t) - z_{v0}(t)} \quad (12)$$

where α_s is the thermal diffusivity of solid.

Combining Eqs.(11) and (12) gives,

$$z'_{v0}(t) = \frac{1}{\rho_l L_v} [I_{abs} + h_g (T_g - T_{l0}) + \frac{k_s T_m (\frac{1}{e} - 1)}{2\sqrt{\alpha_s t}} + \rho_l H_{ox} \eta_{ox} z'_{m0}(t) + \rho_s L_m z'_{m0}(t)] \quad (13)$$

where $z'_{v0}(t) = \frac{dz_{v0}(t)}{dt}$ and $z'_{m0}(t) = \frac{dz_{m0}(t)}{dt}$.

2.2 Mass balance

As the drilling occurs mainly in the vertical direction, it is possible to assume that the mass of the solid melt at the solid-liquid interface is equal to the mass removed due to melt ejection and vaporization, i.e.

$$\dot{m}_s = \dot{m}_v + \dot{m}_m$$

$$S_{sl} \rho_s \frac{\partial z_m}{\partial t} = S_m \rho_l V_m + S_{lv} \rho_l \frac{\partial z_v}{\partial t} \quad (14)$$

where S_{sl} , S_{lv} , S_m , and V_m are the solid-liquid interface area, liquid-vapour interface area, melt ejection area, and the melt ejection velocity, respectively.

For parabolic hole profile, the surface area S_{sl} and S_{lv} are estimated by:

$$S_{sl} = \frac{\pi r_{m0}}{6z_{m0}^2(t)} [(r_{m0}^2 + 4z_{m0}^2(t))^{3/2} - r_{m0}^3] \quad (15)$$

$$S_{lv} = \frac{\pi r_{v0}}{6z_{v0}^2(t)} [(r_{v0}^2 + 4z_{v0}^2(t))^{3/2} - r_{v0}^3] \quad (16)$$

Eq.(14) can now be expressed as:

$$\frac{\pi r_{m0}}{6z_{m0}^2(t)} [(r_{m0}^2 + 4z_{m0}^2(t))^{3/2} - r_{m0}^3] \times$$

$$\left(z'_{m0}(t) - \frac{r^2 z'_{m0}(t)}{r_{m0}^2} \right)$$

$$= \pi(r_{m0}^2 - r_{v0}^2)\rho_l V_m + \frac{\pi r_{v0}}{6z_{v0}^2(t)} [(r_{v0}^2 + 4z_{v0}^2(t))^{3/2} - r_{v0}^3] \rho_l \left(z'_{v0}(t) - \frac{r^2 z'_{v0}(t)}{r_{v0}^2} \right) \quad (17)$$

As $r \rightarrow 0$, the mass equation becomes:

$$\frac{\pi r_{m0}}{6z_{m0}^2(t)} [(r_{m0}^2 + 4z_{m0}^2(t))^{3/2} - r_{m0}^3] \rho_s z'_{m0}(t) = \pi(r_{m0}^2 - r_{v0}^2)\rho_l V_m + \frac{\pi r_{v0}}{6z_{v0}^2(t)} [(r_{v0}^2 + 4z_{v0}^2(t))^{3/2} - r_{v0}^3] \rho_l z'_{v0}(t) \quad (18)$$

However, because Eq.(18) is quite complex, solving the system of equations analytically would be a time consuming process. Therefore, for the sake of simplicity, the paraboloid surface area is approximated here by the conical surface area, which can be formulated in a much simpler form. Collins [18] has also developed a model using both conical and parabolic profiles. The results confirm that there is no significant difference in the hole depth prediction.

The mass balance can now be expressed in term of the conical surface area as:

$$sc r_{m0} \rho_s z'_{m0}(t) \sqrt{r_{m0}^2 + t^2 (z'_{m0}(t))^2} = (r_{m0}^2 - r_{v0}^2) \rho_l V_m + sc r_{v0} \rho_l z'_{v0}(t) \sqrt{r_{v0}^2 + t^2 (z'_{v0}(t))^2} \quad (19)$$

where sc is a surface area correction factor and is taken to be 1.23 in this present model.

Eq.(19) may be rearranged as:

$$z'_{v0}(t) = \frac{1}{\sqrt{2}} \sqrt{\frac{-r_{v0}^4 sc^2 \rho_l^2 + \sqrt{r_{v0}^2 sc^2 \rho_l^2 (a_1 + a_2 + a_3)}}{r_{v0}^2 sc^2 t^2 \rho_l^2}} \quad (20)$$

where

$$a_1 = (r_{v0}^6 sc^2 + 4r_{m0}^4 t^2 V_m^2 - 8r_{m0}^2 r_{v0}^2 t^2 V_m^2 + 4r_{v0}^2 t^2 V_m^2) \rho_l^2, \\ a_2 = 4r_{m0}^4 sc^2 t^2 \rho_s^2 (z'_{m0}(t))^2 + 4r_{m0}^2 sc^2 t^4 \rho_s^2 (z'_{m0}(t))^4, \\ a_3 = 8r_{m0} (-r_{m0}^2 + r_{v0}^2) sc t^2 V_m \rho_l \rho_s z'_{m0}(t) \times \sqrt{r_{m0}^2 + t^2 (z'_{m0}(t))^2}.$$

By equating Eq.(13) to Eq.(20), $z'_{m0}(t)$ and $z'_{v0}(t)$ can now be determined using the Mathematica software as a tool.

The positions of the solid-liquid and liquid-vapour interfaces at $r = 0$ can be determined from

$$z_{m0}(t) = \int_0^t z'_{m0}(t) dt \quad (21)$$

$$z_{v0}(t) = \int_0^t z'_{v0}(t) dt \quad (22)$$

Finally, the solid-liquid and liquid-vapour profiles are obtained from Eqs.(9) and (10).

2.3 Melt front radius at the hole entrance

(r_{m0})

In previously developed laser drilling models, it is often assumed that the hole entrance diameter would not exceed the beam spot diameter [11, 14, 18, 19]. In fact, especially in case of metals, the hole entrance diameter is usually larger than the theoretical beam spot diameter due to radial heat diffusion. Hence, to improve from the previous models, the hole entrance diameter is estimated from the spatial temperature distribution due to an instantaneous point source, which is written as [20]:

$$T_r(r, t) = \frac{P_p}{2\pi\alpha_l \rho_l c_{pl} t} \exp\left(\frac{-r^2}{4\alpha_l t}\right) \quad (23)$$

where T_r and P_p are temperature distribution in the radial direction and laser peak power.

The melt front radius at the hole entrance (r_{m0}) is hence approximated by a radial distance at which $T_r = T_m$.

2.4 Melt ejection velocity (V_m)

From Eq.(20), value of the melt ejection velocity is required. It may be determined by using Bernoulli's equation:

$$p_{vap} + p_{eff} = \frac{\rho_l V_m^2}{2} + \rho_l g z_{m0}(t) + \frac{\sigma}{r_b} \quad (24)$$

where p_{vap} , p_{eff} , g and σ are vapour pressure, effective assist gas pressure, gravitational acceleration and surface tension, respectively. The hydrostatic and surface tension terms on the right-hand side are negligible compared other terms. Therefore, the expression for melt ejection velocity is written as:

$$V_m = \sqrt{\frac{2(p_{vap} + p_{eff})}{2\rho_l}} \quad (25)$$

Therefore, to obtain a value for the melt ejection velocity, values of the vapour pressure,

p_{vap} , and the effective assist gas pressure, p_{eff} , are essential.

2.5 Vapour pressure (p_{vap})

Vapour pressure exerted on the melt surface can be estimated from the Clausius-Clapeyron equation [21, 22]:

$$p_{vap} = p_0 \exp \left[\frac{L_v}{R} \left(\frac{1}{T_b} - \frac{1}{T_{l0}} \right) \right] \quad (26)$$

where p_0 and T_b are atmospheric pressure and boiling temperature, R is the specific gas constant which is taken as 149.13 J/kg.K for steel.

2.6 Effective assist gas pressure (p_{eff})

In addition to supplying exothermic energy to the process, assist gas also contributes to melt ejection mechanism. By adding the assist gas pressure to the recoil pressure exerted on the molten liquid surface, more liquid can be removed and thus producing a higher penetration rate.

For isentropic gas flow, total pressure, which consists of static and dynamic pressure terms, is constant along the gas stream. However, in a case of laser drilling, where the hole bottom is perpendicular to the gas axis, and if a uniform gas pressure profile is assumed within the laser beam, the dynamic gas pressure may be negligible. Due to adiabatic expansion of the assist gas at the nozzle exit, the gas is accelerated up to the local speed of sound leading to the critical state [13, 14]. The critical assist gas pressure at the nozzle exit, p_c , can be defined as:

$$p_c = \left(\frac{2}{\gamma + 1} \right)^{\frac{\gamma}{\gamma - 1}} p_i \quad (27)$$

where p_i is the pressure inside the nozzle, γ is the specific heat ratio which is taken to be 1.4 for oxygen assist gas.

At the hole entrance, assist gas pressure is reduced from p_c to p_{eff} due to pressure loss between the gas nozzle exit and the hole entrance.

$$p_{eff} = p_c \frac{A_{eff}}{A_{eff} + A_{rl}} \quad (28)$$

where A_{eff} is the effective area of gas entering the hole, A_{rl} is the cylindrical area of radial loss of assist gas pressure defined by the nozzle exit diameter, d_n , and nozzle-workpiece distance, z_n :

$$A_{eff} = \pi r_b^2 \quad (29)$$

$$A_{rl} = \pi d_n z_n \quad (30)$$

3. Physical properties

The thermophysical properties of the low carbon steel and assist gas are given in Tables 1 and 2.

Table 1 Thermophysical properties of low carbon steel [23].

Physical properties	
Density of solid, ρ_s (kg m ⁻³)	7800
Density of liquid, ρ_l (kg m ⁻³)	6980
Specific heat of solid, c_{ps} (J kg ⁻¹ K ⁻¹)	628
Specific heat of liquid, c_{pl} (J kg ⁻¹ K ⁻¹)	748
Thermal diffusivity of solid, α_s (m ² s ⁻¹)	0.014 × 10 ⁻³
Thermal diffusivity of liquid, α_l (m ² s ⁻¹)	0.007 × 10 ⁻³
Latent heat of melting, L_m (J kg ⁻¹)	276 × 10 ³
Latent heat of vaporization, L_v (J kg ⁻¹)	6088 × 10 ³
Initial temperature, T_0 (K)	300
Melting temperature, T_m (K)	1808
Boiling temperature, T_b (K)	3100

Table 2 Thermophysical properties of O₂ assist gas [24-26] and gas nozzle parameters.

O ₂ properties	
Density of gas, ρ_g (kg m ⁻³)	1.3007
Viscosity of gas, μ_g (N s m ⁻²)	2.01 × 10 ⁻⁵
Thermal conductivity, k_g (W m ⁻¹ K ⁻¹)	0.0259
Prandtl number, Pr	0.73
Assist gas nozzle exit diameter, d_n (m ²)	1.5 × 10 ⁻³
Nozzle-workpiece distance, z_n (m)	5.8 × 10 ⁻³

4. Results and discussion

In this section, the results for hole depth and hole profile are presented and discussed. Fig. 2 shows the evolution of hole depth as a function of number of pulses for the cases of 1.0 and 1.5 ms pulse width. These results indicate that the hole depth increases sharply during the interaction with the first laser pulse. In other words, maximum drilling speed per pulse is obtained with the first pulse. The subsequent laser pulses propagate into the workpiece at an approximately constant speed. The recession of the drilling speed can be attributed to the fact that once the cavity is generated, vapour formed above the liquid surface may absorb and block part of laser energy resulting in beam scattering and causing less energy being delivered to the workpiece, hence lowering penetration rate. It can also be seen from Fig. 2 that the longer pulse width produces the deeper hole. This is due to more laser energy is delivered to the workpiece.

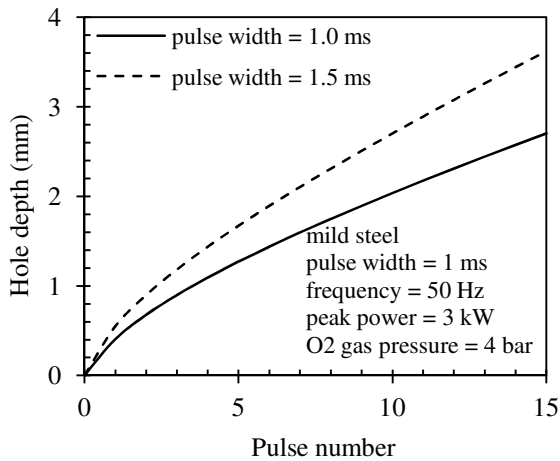


Fig. 2 Hole depth prediction

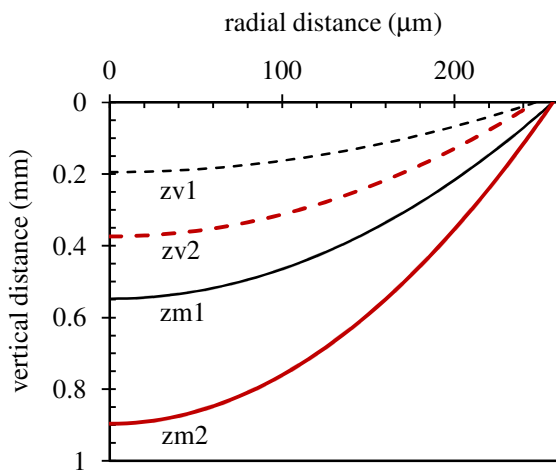


Fig. 3 Hole profiles

Fig. 3 illustrates the predicted profiles of solid-liquid and liquid-vapour interfaces after irradiating with 1 and 2 pulses. The horizontal axis represents the radial distance from the hole symmetry line whereas the vertical axis represents the vertical distance from the workpiece surface. The hole profiles plotted in this figure are for the case of blind holes. Fig. 3 shows that once a keyhole has been produced by the first pulse, subsequent laser pulses enlarge the hole wall, hence resulting in smaller hole taper.

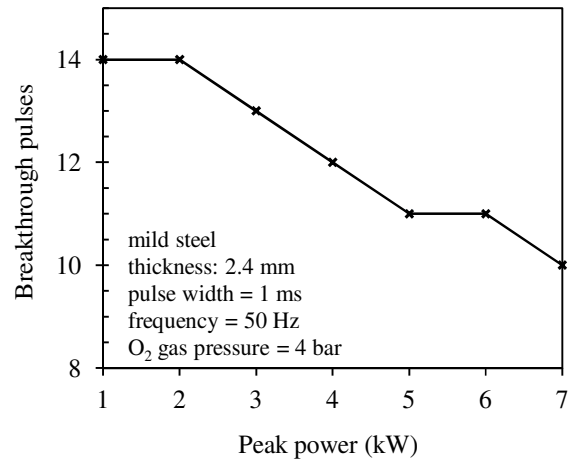


Fig.4 Effects of peak power on breakthrough pulses

In Fig. 4, number of pulses required to initiate the breakthrough are plotted at various peak power values. At high peak power, more laser energy is absorbed by the workpiece resulting in higher penetration rate. Therefore, less pulse is required to produce a through hole. However, for any two adjacent values of the peak power, the difference in the breakthrough pulse may be not obvious, for example 1 and 2 kW and 5 and 6 kW in Fig. 4.

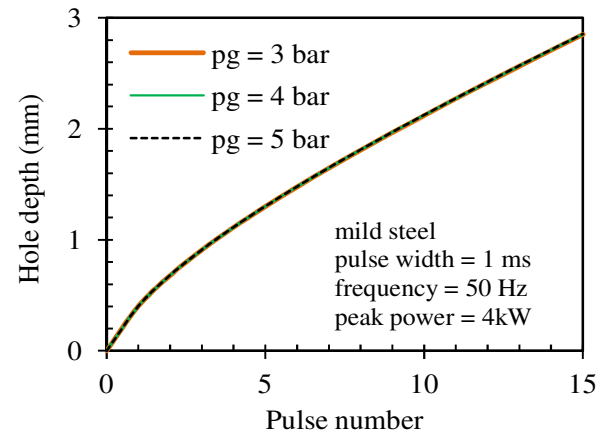


Fig. 5 Effects of assist gas pressure on melt depth

Fig. 5 shows the hole depth evolutions calculated using 3, 4, and 5 bar assist gas pressure in the model. It can be seen that assist gas pressure alone has no significant impact on the melt depth. Calculations show that oxygen assist gas has more pronounced effects on producing exothermic energy to the process rather than adding the pressure to the recoil pressure.

5. Conclusion

This paper presents a new mathematical model of laser percussion drilling incorporating the effects of: (i) exothermic reaction, (ii) assist gas pressure, and (iii) recoil pressure into the model. Assuming that the solid-liquid and liquid-vapour interfaces have parabolic profiles, the model enables the prediction of the hole depth and hole profile. The results obtained from the model show that:

- (1) For laser percussion drilling, the drilling rate rises sharply in the beginning and becomes slower as the number of laser pulses increase. Subsequent laser pulses, however, play a more important role in enlarging the hole at the exit.
- (2) The increase in pulse width and peak power results in a deeper hole.
- (3) Assist gas pressure has no significant influence on the hole depth.

6. References

- [1] C.Y.Yeo, S.C.Tam, S.Jana, and M.W.S.Lau, "A Technical Review of the Laser Drilling of Aerospace Materials," *Journal of Materials Processing Technology*, vol. 42, pp. 15-49, 1994.
- [2] A.Corcoran, L.Sexton, B.Seaman, P.Ryan, and G.Byrne, "The Laser Drilling of Multi-Layer Aerospace Material Systems," *Journal of Materials Processing Technology*, vol. 123, pp. 100-106, 2002.
- [3] C.A.McNally, J.Folkes, and I.R.Pashby, "Laser Drilling of Cooling Holes in Aeroengines: State of the Art and Future Challenges," *Materials Science and Technology*, vol. 20, pp. 805-813, 2004.
- [4] J.J.Benes, "Technology Adds a New Twist to Difficult Drilling," *American Machinist*, vol. 140, pp. 78-79, 1996.
- [5] K.T.Voisey and T.W.Clyne, "Laser Drilling of Cooling Holes through Plasma Sprayed Thermal Barrier Coatings.," *Surface & Coatings Technology* vol. 176, pp. 296-306, 2004.
- [6] N.B.Dahotre and S.P.Harimkar, *Laser Fabrication and Machining of Materials*: Springer Science+Business Media, LLC, 2008.
- [7] L.Li, "The Challenges ahead for Laser Macro, Micro, and Nano Manufacturing," in *Advances in Laser Materials Processing : Technology, Research and Applications*, J.Lawrence, J.Pou, D.K.Y.Low, and E.Toyserkani, Eds., ed: Boca Raton : CRC Press ; Oxford : Woodhead Pub, 2010.
- [8] F.Dausinger, "Laser Drilling with Short Pulses," *Proceedings of SPIE*, vol. 4184, pp. 519-524, 2001.
- [9] S.I.Anisimov, "Vaporization of Metal Absorbing Laser Irradiation," *Soviet Physics-JETP*, vol. 27, p. 182, 1968.
- [10] M.V.Allmen, "Laser Drilling Velocity in Metals," *Journal of Applied Physics*, vol. 47, pp. 5460-5463, 1976.
- [11] A.Kar, T.Rockstroh, and J.Mazumder, "Two-Dimensional Model for Laser-Induced Materials Damage: Effects of Assist Gas and Multiple Reflections inside the Cavity," *Journal of Applied Physics*, vol. 71, pp. 2560-2569, 1992.
- [12] Z.H.Shen, S.Y.Zhang, J.Lu, and X.W.Ni, "Mathematical Modeling of Laser Induced Heating and Melting in Solids," *Optics and Laser Technology*, vol. 33, pp. 533-537, 2001.
- [13] G.K.L.Ng, P.L.Crouse, and L.Li, "An Analytical Model for Laser Drilling Incorporating Effects of Exothermic Reaction, Pulse Width and Hole Geometry," *International Journal of Heat and Mass Transfer*, vol. 49, pp. 1358-1374, 2006.
- [14] D.K.Y.Low, L.Li, and P.J.Byrd, "Hydrodynamic Physical Modeling of Laser Drilling," *Transactions of the ASME*, vol. 124, pp. 852-862, 2002.
- [15] J.Dowden and P.Kapadia, "The Penetration Depth in Keyhole Welding with Pseudo-Continuous Nd-YAG and CO Lasers Investigated Mathematically," *Applied Surface Science*, vol. 106, pp. 235-239, 1996.
- [16] D.Lacroix, A.G.Jeandel, and C.Boudot, "Spectroscopic Characterization of Laser-Induced Plasma Created during Welding with a Pulsed Nd:YAG Laser," *Journal of Applied Physics* vol. 81, pp. 6599-6606, 1997.
- [17] R.E.Wagner, "Laser Drilling Mechanics," *Journal of Applied Physics*, vol. 45, pp. 4631-4637, 1974.
- [18] J.Collins and P.Gremaud, "A Simple Model for Laser Drilling," *Mathematics and*

- Computers in Simulation*, vol. 81, pp. 1541-1552, 2011.
- [19] A.Kar and J.Mazumder, "Two-Dimensional Model for Material Damage due to Melting and Vaporization during Laser Irradiation," *Journal of Applied Physics*, vol. 68, pp. 3884-3891, 1990.
- [20] H.S.Carslaw and J.C.Jaeger, *Conduction of Heat in Solids*. Newyork: Oxford University Press, 1959.
- [21] D.A.McQuarrie and J.D.Simon, *Physical Chemistry - A Molecular Approach*. Sausalito, Calif: University Science Books, 1997.
- [22] P.W.Atkins, *Physical Chemistry*, 7th ed. Oxford: Oxford University Press, 2002.
- [23] V.Semak and A.Matsunawa, "The Role of Recoil Pressure in Energy Balance during Laser Materials Processing," *Journal of Physics D: Applied Physics*, vol. 30, pp. 2541-2552, 1997.
- [24] Y.S.Touloukian, P.E.Liley, and S.C.Saxena, "Thermophysical Properties of Matter: Thermal Conductivity ". vol. 3, Y.S.Touloukian and C.Y.Ho, Eds., ed New York: IFI/Plenum, 1970.
- [25] Y.S.Touloukian, S.C.Saxena, and P.Hestermans, "Thermophysical Properties of Matter: Viscosity." vol. 11, Y.S.Touloukian and C.Y.Ho, Eds., ed New York: IFI/Plenum, 1970.
- [26] P.E.Liley, *Properties of Nonmetallic Fluid Elements, McGraw-Hill/CINDAS Data Series on Material Properties* vol. III-2. New York: McGraw-Hill, 1981.